geosciences

MDPI

Supplementary Materials

1. Details of FCT measurements

At XFM, filtered pink beam was focused by achromatic Kirkpatrick-Baez (KB) mirrors to 1 μm at the sample position. The pink beam consisted of a broad spectrum from approximately 12 to 20 keV; the lower bound is defined by a 1 mm thick Al filter, and the upper bound determined by reflectivity of Rh-coated mirror optics. The sample was secured to a fused silica post and mounted to a fast-scanning translation and rotation stage (Fig. S1). FCT measurements of each slice were accomplished by repeatedly rastering the sample across the focused beam at increments of rotation while recording fluorescence intensities with a Canberra SXD 7-element silicon drift detector coupled to Quantum Detectors Xspress3 electronics; the detector was filtered with 2 layers of 4 mil Kapton film; detector was oriented at 90 degrees to incident beam for optimal fluorescence measurement. Data for slices 30 to 33 were collected using 4 μm horizontal pixel size, 0.6 degree rotational increments and 50 ms dwell time per pixel, yielding a 4x4x1 μm voxel size; slices 32 and 33 were repeated using 2 μm horizontal pixel size, 0.3 degree rotational increments and 100 ms dwell time, yielding a 2x2x1 μm voxel size. Reconstructions employing a conventional filtered back projection algorithm were processed using a tomo-Py plugin to GSE Mapviewer in the LARCH software package [32]. Measured concurrently with fluorescence, transmission through the sample provides a measure of absorption contrast. Advantages of pink beam over monochromatic beam FCT are higher brightness for better spatial resolution and speed, efficient stimulation of a wider range of elements, and more detailed absorption contrast with wider dynamic range.

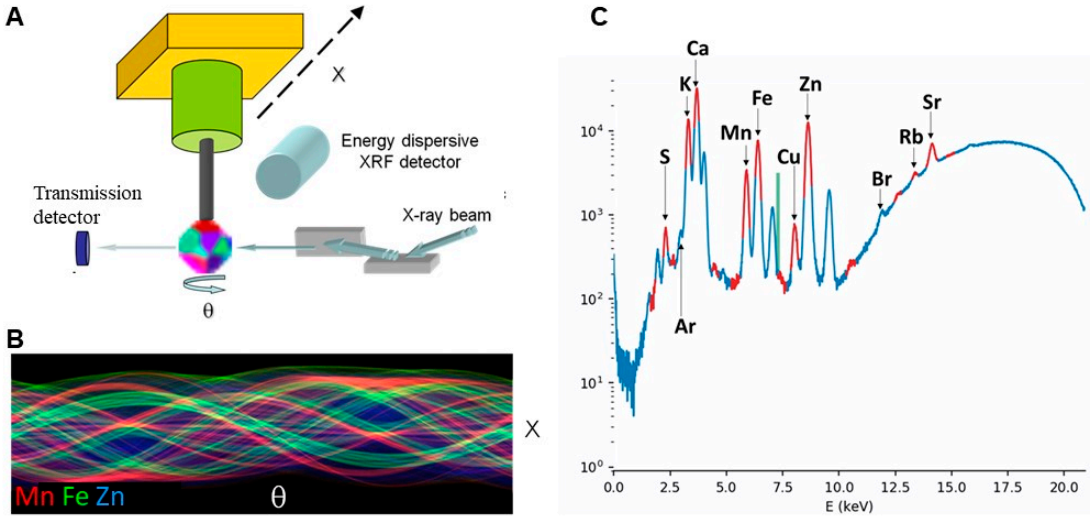

Figure S1. **a.** Schematic of FCT instruments. Incident beam, from right to left, is focused to microbeam spot size at the sample position; sample is rastered in x at 45 degrees to beam, and rotated about an axis perpendicular to both x and incident beam; fluorescence is measured by detector positioned at 90 degrees to incident beam; transmission through the sample is measured by photodiode downstream. **b.** An example of a sinogram, the raw data for three selected elements as measured in terms of x and theta before tomographic reconstruction. **c.** An example fluorescence spectrum stimulated by filtered pink beam at XFM, in log scale. Note the increase in background between ~12 and 20 keV due to scatter of the incident pink beam.

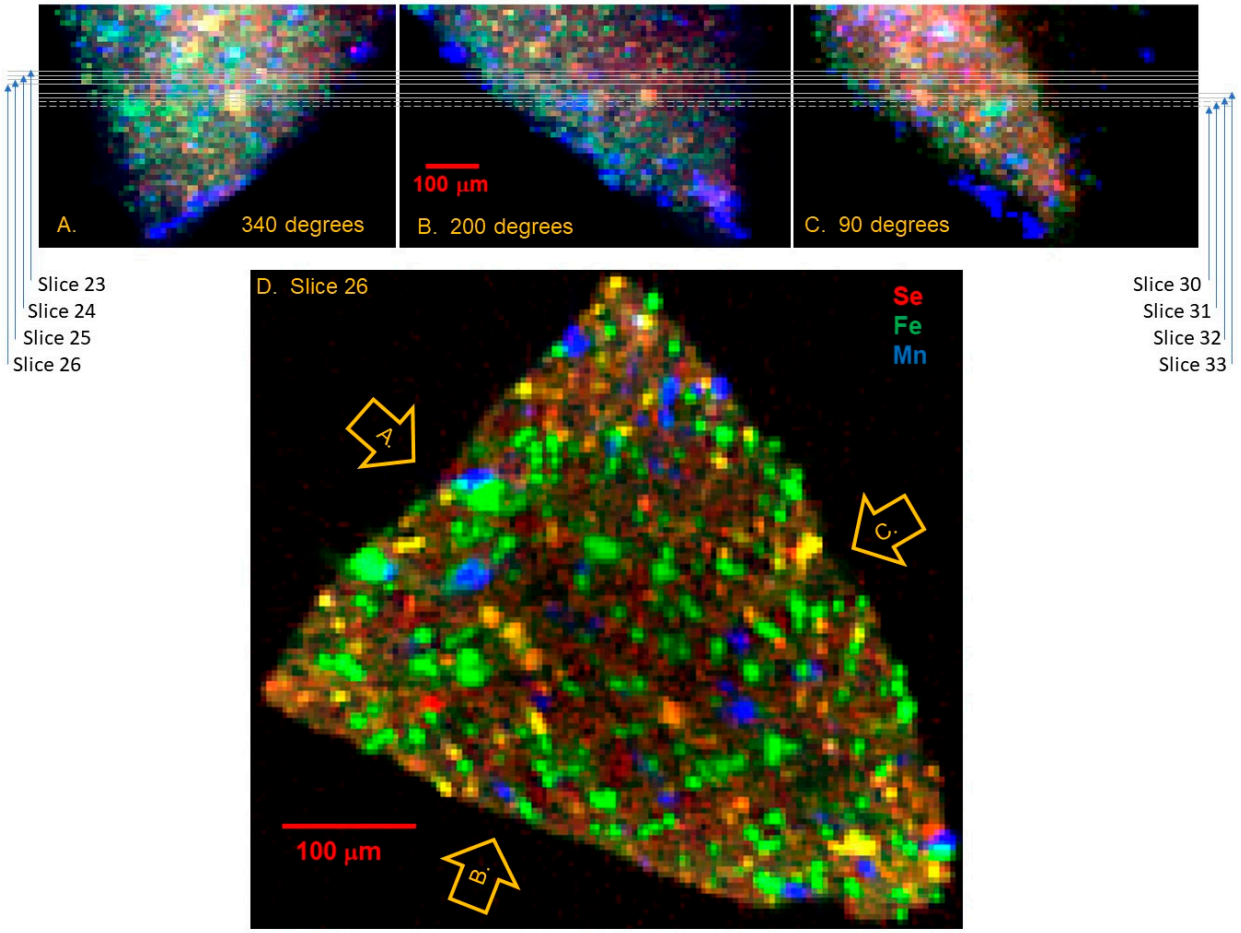

Figure S2. Geometry of pink-beam FCT of sample C0034. The fragment measured for this study was crudely bipyramidal in shape with triangular cross-section, as fully shown in Fig. 7. **a,b,c.** Microbeam XRF 2-D maps of the tapered tip of the grain, of roughly flat surfaces oriented at 340, 200 and 90 degree positions, illuminated with pink microbeam. False-color composite maps indicate relative XRF intensities for Se in red, Fe in green, and Mn in blue. Pixel size is 10 µm. In these views, linear traces indicate z-positions of tomographic slices reported here, z is vertical. **d.** Reconstructed FCT virtual slice 26, shown in the same false colors. 3-D voxel size is 4 x 4 µm in the plane of the slice x 1 µm thick. Arrows labeled A, B and C indicate the surfaces mapped in (a), (b) and (c), respectively. Consecutively numbered slices are 10 µm apart in z.

As shown in Fig. S2d, the tomographic slice has a cleaner representation of discrete components than the surface maps shown in Figs. S2a-c, in which the sampling depth is tens of µm and images show overlap of different grains from depth. The element-specific maps in conjunction with absorption contrast, in a 1-µm thick virtual slice, enable interpretation of phases and semi-quantitative compositional analysis of individual grains inside the sample. Raw unreconstructed FCT data are available on request from the corresponding author.

2. Details of XANES analyses

In the Ca XANES of rhombohedral carbonates, spectral features are highly sensitive to local coordination and can differentiate between host phases. Detailed analysis is presented in Fig. S3 and Table S1.

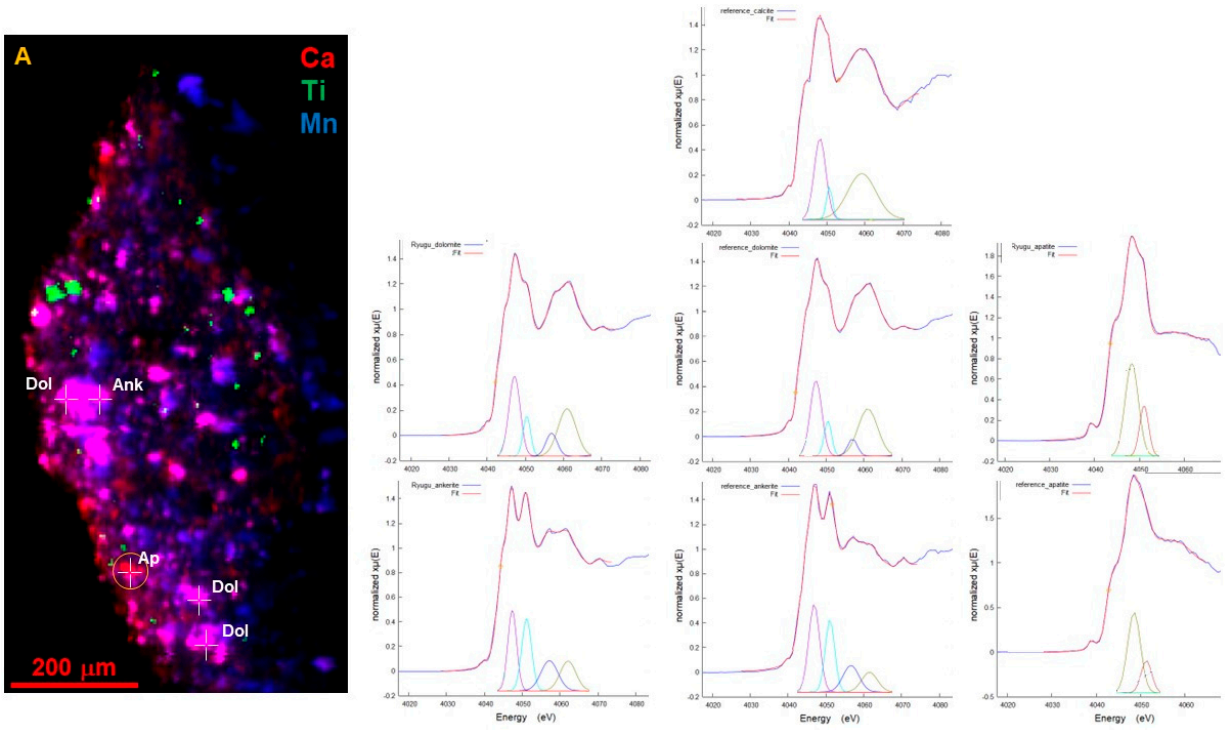

Figure S3. Calcium μXANES spectral feature analysis. **a.** Tender energy XRF map of C0034 fragment as shown in Fig. 4c, annotated by crosses marking specific locations of Ca μXANES spot measurements at XFM. Phases identified by XANES are labeled Dol (dolomite), Ank (ankerite) and Ap (apatite). **b.** XANES spectral feature analyses: data shown in blue, fit of constituent features shown in red. Key diagnostic peaks are plotted below the spectrum; these confirm the match of C0034 component grains with references dolomite, ankerite and apatite. See Table S1 for determined peak positions. Note the progression of increased peak separations from calcite to dolomite to ankerite.

Table S1. Key diagnostic peak positions (in eV) determined from Ca μXANES spectral feature analyses shown in Fig. S3.

Sample	peak a	peak b	peak c	peak d	fit R-factor
reference calcite	4048.02(7)	4050.5(2)	4059.1(1)	--	0.0003
reference dolomite	4047.50(5)	4050.62(9)	4057.1(4)	4061.12(6)	0.0001
C0034 dolomite	4047.41(4)	4050.63(6)	4057.1(3)	4061.22(4)	0.0001
reference ankerite	4047.0(4)	4051.15(10)	4056.7(5)	4061.6(2)	0.0002
C0034 ankerite	4047.1(2)	4050.88(4)	4056.9(3)	4061.79(8)	0.0002
reference apatite	4048.27(10)	4051.0(3)	--	--	0.0003
C0034 apatite	4048.21(3)	4050.92(6)	--	--	0.0002

Sulfur XANES can easily differentiate between sulfide and sulfate, as there is a >10-eV difference in primary peak position. The primary peak is the result of the favorable 1s-2p electronic transition. In sulfides, this peak is also sensitive to electronic differences between sulfide species. For example, in comparing pyrrhotite to troilite, pyrrhotite is a defect structure (Fe_7S_8), with Fe vacancies relative to troilite FeS. Therefore, some of the S atoms will be under-coordinated by Fe, resulting in fewer but stronger Fe-S bonds. This shifts the peak position for those S atoms, resulting in splitting of the spectral peak into two. Meanwhile, the effective oxidation state of S is slightly more positive in pyrrhotite than the 2- state in troilite. This slightly shifts the absorption edge position (the steep rise around 2475 eV) to higher energy in pyrrhotite. Detailed analysis of S XANES is presented in Fig. S4 and Table S2.

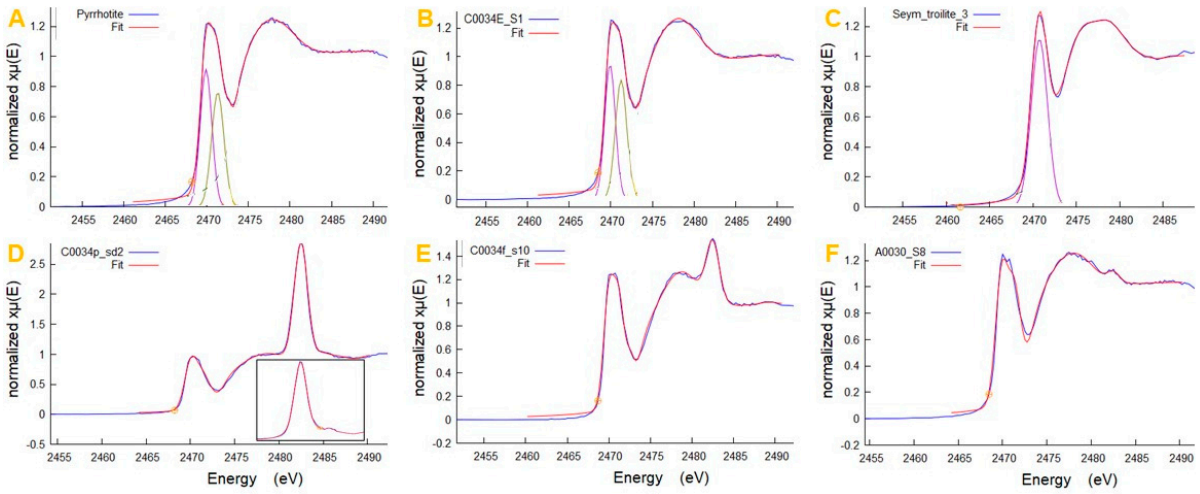

Figure S4. Spectral feature analyses of S μXANES initially shown in Fig. 11, used to identify the sulfide as pyrrhotite and to determine the fraction of S present as sulfate. Data shown in blue, fit of component features shown in red, as in Fig S3. **a.** Reference pyrrhotite highlighting its characteristic double peak. **b.** A representative C0034 sulfide grain exhibiting a closely matching doublet; peak positions given in Table S2. **c.** Reference troilite (Seymchan meteorite) for contrast. **d, e, f.** Analyses of representative Ryugu sulfide grains showing partial oxidation to sulfate. Inset in (d) shows spectrum of reference sulfate in calcite, dominated by a peak at 2482.5 eV. The integrated area of the sulfide peaks, compared to that of the sulfate peak, and corrected for differences in absorption cross-section [15], yields quantitative percentage of sulfate within the volume sampled (in this case 5x5 μm beam spot size x ~2 μm effective sampling depth). Calculated sulfate contents are presented in Table S2.

Table S2. Key peak positions (eV), and relative sulfate percentages, determined from the μXANES spectral feature analyses shown in Fig. S4.

Sample	peak a	peak b	peak c		fit R-factor
reference pyrrhotite	2469.89(5)	2471.30(3)			0.0003
C0034E_s1 pyrrhotite	2469.91(2)	2471.25(2)			0.0004
reference troilite		2470.73(2)			0.0003
reference sulfate in calcite			2482.47(1)		0.0008
				% sulfate	
C0034p_sd2				18.3(2)	0.0008
C0034f_s10				5.0(1)	0.0009
A0030_s8				0.7(1)	0.0008

3. Details of EXAFS analyses

Microbeam EXAFS data for S and Se, in the same sulfide grain in sample C0034, were measured utilizing the TES and XFM beamlines, respectively. This sulfide grain had no significant sulfate component. Pyrrhotite model was from [16]. Fitting to model utilized the full array of first-neighbor S-Fe (Se-Fe) distances, but applied one delta-R and one sigma^2 parameter to all of these distances collectively. This preserved the character of the model but allowed generalized local distortion to accommodate the larger Se. The full set of second-neighbor S-S (Se-S) distances were similarly treated. Using single average values for S-Fe and S-S distances would not preserve the characteristic (non-gaussian) distribution of distances in the pyrrhotite structure. Fitting parameters and results are listed in Table S3.

Table S3. EXAFS fitting parameters and results.

Parameter	**Sulfur**	**Selenium**
k range	1.143 - 8.630	1.288 - 6.498
k-window	hanning	hanning
dk	0.5	0.5
k weight	2	2
R range	1.456 - 3.38	1.0 - 3.4
delta R for S-Fe (Se-Fe)	-0.02(1)	0.10(1)
sigma^2 for S-Fe (Se-Fe)	0.002(1)	0.007(2)
delta R for S-S (Se-S)	0.01(2)	0.03(1)
sigma^2 for S-S (Se-S)	0.002(2)	0.013(4)
R factor	0.024	0.018

4. Additional files

XANES and EXAFS spectra in separate files; file names describe content and match sample names in figures and tables.